LUMINOSITY DEPENDENT CLUSTERING OF STAR-FORMING BzK GALAXIES AT REDSHIFT 2 [1]

Masao Hayashi [2], Kazuhiro Shimasaku [2], Kentaro Motohara [3], Makiko Yoshida [2], Sadanori Okamura [2] and Nobunari Kashikawa [4]
hayashi@astron.s.u-tokyo.ac.jp

ABSTRACT

We use the BzK color selection proposed by Daddi et al. (2004) to obtain a sample of 1092 faint star-forming galaxies (hereafter sBzKs) from 180 arcmin^2 in the Subaru Deep Field. This sample represents star-forming galaxies at $1.4 \lesssim z \lesssim 2.5$ down to $K_{\rm AB} = 23.2$, which roughly corresponds to a stellar-mass limit of $\simeq 1\times10^{10} M_\odot$. We measure the angular correlation function (ACF) of these sBzKs to be $w(\theta) = (0.58 \pm 0.13) \times \theta['']^{-0.8}$ and translate the amplitude into the correlation length assuming a reasonable redshift distribution. The resulting value, $r_0 = 3.2^{+0.6}_{-0.7}$ h^{-1} Mpc, suggests that our sBzKs reside in haloes with a typical mass of $2.8\times10^{11} M_\odot$. Combining this halo mass estimate with those for brighter samples of Kong et al. (2006), we find that the mass of dark haloes largely increases with K brightness, a measure of the stellar mass; the dark halo mass increases by as much as 10^{2-3} as K brightness increases by only a factor of $\simeq 10$. We also find that the halo occupation number, the number of galaxies hosted in a dark halo, is higher for brighter sBzKs. Comparison with other galaxy populations suggests that faint sBzKs ($K_{\rm AB} < 23.2$) and Lyman Break Galaxies at $z \sim 2$ are similar populations hosted by relatively low-mass haloes, while bright sBzKs ($K_{\rm AB} < 21$) reside in haloes comparable to or more massive than those of Distant Red Galaxies and Extremely Red Objects. Using the extended Press-Schechter formalism, we predict that present-day descendants of haloes hosting sBzKs span a wide mass range depending on K brightness, from lower than that of the Milky Way up to those of richest clusters.

Subject headings: cosmology: observations — galaxies: evolution — galaxies: formation — galaxies: high-redshift — galaxies: photometry

1. Introduction

Galaxy mass is probably the most important parameter among those governing the evolution of galaxies. Observations of the local universe show that more massive galaxies tend to have older stellar populations, lower star-formation activities, earlier morphological types, and higher metallicities (e.g., Gallazzi et al. 2005). In Cold Dark Matter (CDM) universes, dark haloes grow with time through merging of less massive haloes, implying that haloes with different masses have different evolutionary histories. Observing galaxies over a wide mass range is thus crucial to place strong constraints on galaxy evolution.

It is extremely difficult to measure dark-halo masses of high-redshift galaxies. One can, however, *infer* them from galaxy clustering on the assumption that galaxies reside in dark haloes, since CDM models predict a monotonic correlation that more massive haloes are clustered more strongly

[1] Based on data collected at Subaru Telescope, which is operated by the National Astronomical Observatory of Japan. Use of the UKIRT 3.8-m telescope for the observations is supported by NAOJ.

[2] Department of Astronomy, Graduate School of Science, University of Tokyo, Tokyo 113-0033, Japan

[3] Institute of astronomy, Graduate School of Science, University of Tokyo, Mitaka, Tokyo 181-0015, Japan

[4] Optical and Infrared Astronomy Division, National Astronomical Observatory, Mitaka, Tokyo 181-8588, Japan

(Mo & White 2002). Measuring galaxy clustering requires a large sample from a wide area.

Recent observations suggest that the era of $z \sim 2$ is important in galaxy evolution for various reasons; the cosmic star formation rate begins to drop at $z \sim 1-2$ from a flat plateau at higher redshifts (Dickinson et al. 2003; Fontana et al. 2003); the morphological type mix of field galaxies changes remarkably at $z \sim 1-2$ (Kajisawa & Yamada 2001); the number density of QSOs has a peak at $z \sim 2$ (Richards et al. 2006). Various color selection methods such as the Lyman-break technique (Guhathakurta et al. 1990) have been proposed so far, in order to construct large samples of galaxies at high redshifts from imaging data. However, color selections for galaxies at $z \sim 2$, the 'redshift desert', have not been as successful as those for other redshifts, mainly because of the lack of distinctive spectral features in the optical wavelength.

Recently, a two-color selection with $B-z'$ and $z'-K$ has been proposed by Daddi et al. (2004) to select galaxies at $1.4 \lesssim z \lesssim 2.5$ effectively with a low contamination. Galaxies selected with this method, referred to as BzKs, make up a good approximation of a sample of all galaxies at $z \sim 2$ down to a limiting magnitude in the K band, roughly equal to a stellar mass limit. Two types of BzKs, sBzKs and pBzKs, are defined according to the position in the $B-z'$ vs $z'-K$ space (Daddi et al. 2004); 's' and 'p' denote star-forming and passive, respectively. It has been shown that most star-forming galaxies at $1.4 \lesssim z \lesssim 2.5$ meet the criteria for sBzKs irrespective of the amount of dust extinction (Daddi et al. 2004).

Previous observations of BzKs have been limited primarily to bright objects with $K < 22$. Those studies have shown that bright sBzKs have star formation rates (SFRs) of $\sim 10^2 M_\odot$ yr^{-1}, stellar masses of $10^{11} M_\odot$, and dust extinctions of $E(B-V) \sim 0.4$ (Daddi et al. 2004, 2005; Kong et al. 2006, hereafter K06). Bright pBzKs are found to have stellar masses of $\gtrsim 10^{11} M_\odot$ with ages of ~ 1 Gyr. Clustering has also been examined recently using samples of bright BzKs from wide-field surveys (K06); both pBzKs and sBzKs are found to be clustered strongly. From these studies, bright BzKs are inferred to be progenitors of the present-day massive galaxies. However, properties of faint, or low-mass, BzKs remain unrevealed due to the difficulty in obtaining deep and wide-field NIR images.

Steidel et al. (2004) have proposed another method to select galaxies at $z \sim 2$ (see also Adelberger et al. 2004). This method uses U, G and R photometry to select far-UV bright star-forming galaxies, referred to as BXs/BMs. Clustering properties of BXs/BMs have been studied using large samples (Adelberger et al. 2005), since NIR imaging is not required. Note, however, that this method will miss dusty galaxies and passive galaxies, both of which are faint in far-UV wavelengths.

We have been conducting a deep survey of BzKs in the Subaru Deep Field (Kashikawa et al. 2004; Maihara et al. 2001) to study properties of faint, or low-mass, BzKs. Details of our survey and the photometric properties of BzKs detected from our survey, such as number densities, star-formation rates, and stellar masses, will be presented elsewhere (Motohara et al. in prep).

In this paper, we report results of clustering analysis of sBzKs detected in our initial data set over 180 arcmin^2. Our study provides the first measurements of angular correlation of faint ($K < 23.2$) sBzKs. Unfortunately, the number of pBzKs in the present sample is not large enough to obtain reliable measurements of their angular correlation. Combining our result with those for bright ($K < 22$) sBzKs given in K06, we examine properties of dark haloes hosting sBzKs over a wide range of K magnitude, or, equivalently, stellar mass. Dark-halo masses are inferred from observed correlation lengths through an analytic model for the spatial clustering of dark haloes (e.g., Mo & White 2002). We also compare the dark-halo masses of sBzKs with those of other populations such as Lyman-break galaxies (LBGs).

The structure of this paper is as follows. The optical and near-infrared data used to select BzKs are described in §2. In §3, we construct a sample of faint sBzKs and check its consistency by comparing it with other samples. We measure the angular correlation function of sBzK in our sample in §4. Then, for both our sample and K06's, the amplitude of the angular correlation function is transformed into the spatial correlation length. Results and discussion are presented in §5, and conclusions are given in §6.

Throughout this paper, magnitudes are in the AB system, and we adopt cosmological parameters of $\Omega_{m0} = 0.3$, $\Omega_{\Lambda 0} = 0.7$. and $\sigma_8 = 0.9$. We assume $h = 0.7$ to compute the power spectrum of the cosmological density fluctuations and physical quantities except the correlation length, where h is the Hubble constant in units of 100 km s^{-1} Mpc^{-1}. The correlation length is expressed in units of h^{-1}Mpc, since most of the previous studies adopted $h = 1$.

2. Data

2.1. Optical Data

The Subaru Deep Field (SDF) is a blank field centered on $(13^h24^m38^s.9, +27°29'25''.9)$ (J2000). The SDF has deep and wide-field Subaru/Suprime-Cam data of seven optical bandpasses, B, V, R, i', z', NB816, and NB921, obtained for the Subaru Deep Field Project (Kashikawa et al. 2004). In this paper, we combine the B and z' data with the K data described below, to select BzK galaxies. The exposure time and the 3σ limiting magnitude on a $2''$ aperture are 595 min and 28.45 mag for B and 504 min and 26.62 mag for z', respectively. Both images have been convolved to a seeing size of $1''.14$ (FWHM), the value for the final J and K images (see below), and have an identical sky coverage of $29'.7 \times 36'.7 = 1090$ arcmin^2 with a pixel scale of $0''.202$ pixel^{-1}.

2.2. Near-Infrared Data

We observed the SDF in the J and K bands with the wide-field camera (WFCAM) on the United Kingdom Infra-Red Telescope (UKIRT) on 2005 April 14 – 15. WFCAM is composed of four 2048×2048-pixel detectors with a large spacing of 12.3 arcmin. Each detector covers $\simeq 13' \times 13'$ of sky with a pixel scale of $0''.4$. We made only a single pointing for each passband to go significantly deeper than the previous wide-field K data used to study BzK galaxies.

Figure 1 shows the sky area of the SDF imaged with Suprime-Cam and WFCAM. The Suprime-Cam $29'.7 \times 36'.7$ field is outlined by the thin solid line. The four dotted rectangles correspond to the regions imaged with the four detectors of WFCAM. The large spacing between the detectors prevented us from covering the Suprime-Cam field effectively. The total area overlapping with the Suprime-Cam field amounts, however, to 410 arcmin^2, large enough to measure the angular clustering of faint BzK galaxies.

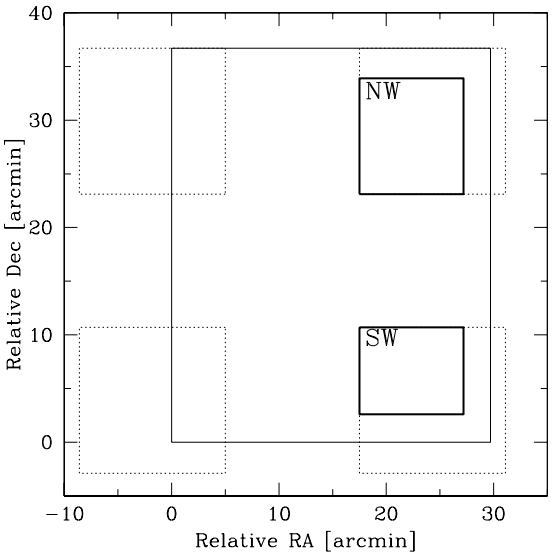

Fig. 1.— The sky area of the SDF observed with Suprime-Cam and WFCAM. The thin solid lines outline the $29'.7 \times 36'.7$ area imaged with Suprime-Cam (B, z'). The four dotted rectangles correspond to the four fields with WFCAM J and K data. we used in this study only the two subregions enclosed with thick solid lines in the northwest and southwest fields.

The exposure time was 150 min for J and 294 min for K. The variations in sensitivity and PSF among the four detectors were found to be small. The seeing size in the final images varied from $1''.04$ to $1''.14$ in K.

Data reduction was made in the standard manner for NIR imaging data, but special care was taken to exclude spurious objects due to crosstalk of bright objects. All the images, except the one with the worst seeing size, were smoothed with a Gaussian kernel so that their PSF sizes be $1''.14$ FWHM. The 2MASS catalog (Skrutskie et al. 2006) was used to conduct astrometry and to derive the magnitude zero point.

We measure the 5σ limiting magnitude on a $2''$-diameter aperture for each detector. The shallowest (brightest) limiting magnitude among the

four detectors is 23.3 mag in J and 23.5 mag in K. The variation in limiting magnitude among the four detectors is less than 0.2 mag for both bandpasses. Details of our observation and data reduction will be described elsewhere (Motohara et al. in prep).

2.3. K-Selected Catalog

Object detection and photometry are made using SExtractor 2.1.3 (Bertin & Arnouts 1996). The K-band is chosen as the detection band. For each object detected in the K image, $2''$-diameter magnitude is measured for B and z' using double-image mode of SExtractor to derive colors. If an object is undetected (fainter than the 2σ magnitude) in B or z', its magnitude is replaced with the 2σ magnitude. We limit our catalog to $K = 23.5$, the shallowest 5σ limiting magnitude among the four detectors. We have in total 8884 objects in the overlapping fields (see Figure 1). The catalog thus constructed is then corrected for Galactic extinction using the dust map of Schlegel et al. (1998): $A(B) = 0.07$ mag, $A(z') = 0.02$ mag, and $A(K) = 0.01$ mag.

2.4. Detection Uniformity

Clustering analysis requires high uniformity in object detection over the image for all passbands, since a variation in detection completeness may produce spurious clustering signals. While the WFCAM J and K images are very uniform, sky noise at the four edges of the Suprime-Cam images is systematically large and non-uniform because of dithered pointing with large angles.

We examine detection uniformity for each of the four overlapping fields by dividing the field into a few dozen of sub-areas and estimating the sky noise in each sub-area for B, z', and K. On the basis of these noise maps, we find that the two subregions surrounded by thick solid lines in Figure 1 have a good detection uniformity in all three passbands. These subregions are well within the good S/N area defined in Kashikawa et al. (2004). In what follows we call these two subregions the NW and SW subregions. The area of NW and SW subregions are 100 arcmin^2 and 80 arcmin^2, respectively.

In this paper, we examine angular clustering only in the NW and SW subregions. Among the 8884 objects found in the four overlapping fields, 3961 are included in these two subregions. The two eastern fields have also sub-areas with a good detection uniformity, but they are all too small for clustering analysis.

3. BzK Galaxies in the Subaru Deep Field

3.1. Selection of BzK Galaxies

In the $B - z'$ vs $z' - K$ plane, sBzKs are defined to be objects with $(z' - K) - (B - z') > -0.2$, while the criteria for pBzKs are defined as $(z' - K) - (B - z') < -0.2 \cap z - K > 2.5$ (Daddi et al. 2004). Stars and foreground galaxies are separated well from BzK galaxies in this plane (Daddi et al. 2004). We also regard objects with $K < 18 \cap$ CLASS_STAR > 0.9 as stars, where CLASS_STAR is the stellarity index parameter from SExtractor. Although the validity of the BzK selection for objects fainter than $K \simeq 22$ has not been examined well, we assume that the selection and the classification into two types are applicable to our objects as well.

In the selection of BzKs, special care is required for objects undetected in B or z', i.e., $B > B_{2\sigma\,\mathrm{lim}}$ or $z' > z'_{2\sigma\,\mathrm{lim}}$, where $B_{2\sigma\,\mathrm{lim}}$ and $z'_{2\sigma\,\mathrm{lim}}$ are the 2σ limiting magnitudes. We treat these objects as follows:

- Objects undetected in B but detected in z'. If their $B_{2\sigma\,\mathrm{lim}} - z'$ and $z' - K$ colors meet the pBzK criteria, they are classified as pBzKs, since their true $B - z'$ colors, which are redder than $B_{2\sigma\,\mathrm{lim}} - z'$, also meet $(z' - K) - (B - z') < -0.2$. On the other hand, classification is not applied to those whose $B_{2\sigma\,\mathrm{lim}} - z'$ and $z' - K$ colors satisfy the sBzK criterion, since their true $B - z'$ colors may be too red to be classified as sBzKs.

- Objects detected in B but undetected in z'. If their $B - z'_{2\sigma\,\mathrm{lim}}$ and $z'_{2\sigma\,\mathrm{lim}} - K$ colors meet the sBzK criterion, they are classified as sBzKs, since they do not go out of the sBzK region even when true z' magnitudes, which are fainter than $z'_{2\sigma\,\mathrm{lim}}$, are used instead. On the other hand, classification is not applied to those with $B - z'_{2\sigma\,\mathrm{lim}}$ and $z'_{2\sigma\,\mathrm{lim}} - K$ satisfying the pBzK criteria, since their true $B - z'$ may be too blue to be classified as pBzKs.

- Objects undetected in both B and z'. These objects are not classified, because their $B - z'$ colors can take any values.

The numbers of sBzKs and pBzKs selected are 1092 and 56, respectively (Table 1). Figure 2 shows the $B - z'$ vs $z' - K$ distribution of all objects in the NW and SW subregions.

Our B, z', and K bandpasses are not exactly the same as those originally used to define the BzK selection criteria in Daddi et al. (2004). We use Gunn & Stryker (1983)'s stellar spectrophotometric atlas to find that the $B - z'$ colors of stars defined in our system can be bluer than those in Daddi et al. (2004) up to 0.2 mag, depending on the spectral type, while there is little difference in $z' - K$. We also make a similar evaluation using the spectral templates of local galaxies (E to Im) given in Coleman et al. (1980) redshifted to $z \sim 2$. It is found that the $B - z'$ colors of these galaxies in our system are at most 0.1 mag bluer than those in Daddi et al. (2004) while our $z' - K$ colors are at most 0.1 mag redder.

These results imply that applying the original sBzK boundary, $(z' - K) - (B - z') > -0.2$, to our data will select additional objects near the boundary which, if measured in the system of Daddi et al. (2004), may not be selected. Our sBzK sample will be reduced by $\simeq 15$ % when the selection boundary is tightened by 0.2 mag (i.e., $(z' - K) - (B - z') > 0.0$). This reduction should be an upper limit to the effect of the bandpass differences, since the net offset in the $B - z'$ vs $z' - K$ plane of sBzKs due to the bandpass differences will be on average more modest than 0.2 mag. Because this reduced sample gives a very similar ACF, we have decided not to adjust the selection boundary in our study.

We find that the 2″-aperture K magnitudes of our BzKs are on average 0.3 mag fainter than the total magnitudes (we adopt MAG_AUTO magnitudes for total magnitudes). For this reason, we regard that our BzK sample is flux-limited to a total magnitude of $K = 23.2 (= 23.5 - 0.3)$.

Table 1: Numbers of sBzKs, pBzKs and unclassified objects

Detection*		sBzK	pBzK	unclassified
B	z'			
○	○	1092	40	0
×	○	0	16	20
○	×	0	0	0
×	×	0	0	9
total		1092	56	29

* ○ and × represent detection and non-detection, respectively.

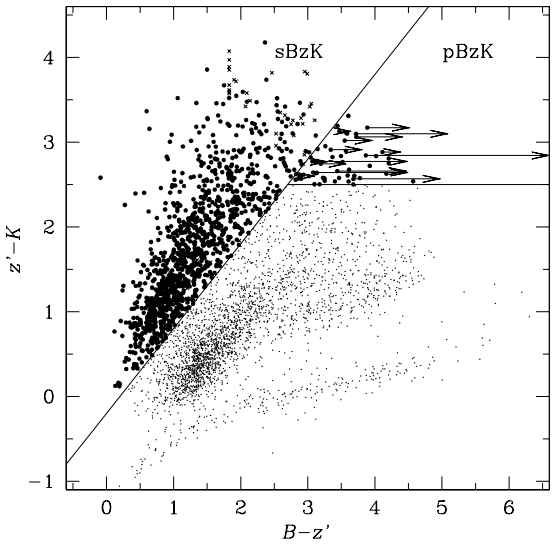

Fig. 2.— $B-z'$ vs $z'-K$ distribution of all objects in the NW and SW subregions. For objects undetected in B or z', $B_{2\sigma\,\mathrm{lim}}$ and $z'_{2\sigma\,\mathrm{lim}}$ have been used, respectively, in the plot. Filled circles represent BzKs; those with a horizontal arrow are undetected in B. Crosses represent unclassified objects.

3.2. Number Counts

Figure 3 compares the number counts of sBzKs, pBzKs, and all galaxies from our data with those given by K06. Since K06's data are from two wide fields, EIS Deep3A field and Daddi field, we plot the counts from these two fields separately. It is found that our number counts of sBzKs and all galaxies are consistent with those of K06 while pBzK are lower by a factor of 2 - 3. This disagreement in the number counts of pBzK may be partly due to cosmic variance. Indeed, even in the two fields surveyed by K06, both of which are sev-

eral times larger than our total area, the counts are different significantly. A small part of the disagreement may also result from our special treatment in the BzK selection for objects undetected in B or z' described in Section 3.1, which has not been considered in K06.

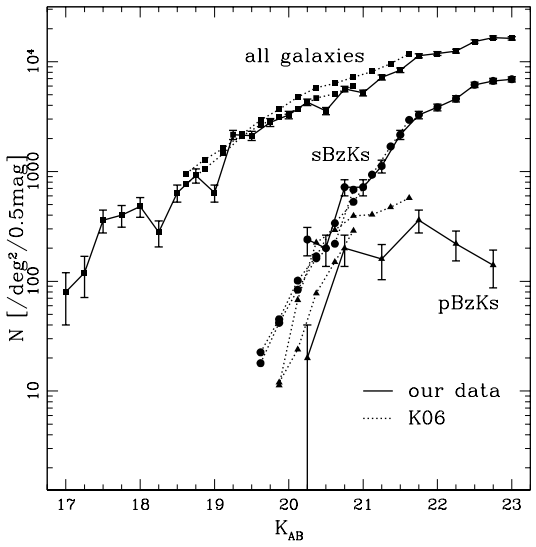

Fig. 3.— Number counts of sBzKs, pBzKs, and all galaxies as a function of total magnitude (MAG_AUTO). The circles, triangles, and squares represent sBzKs, pBzKs, and all galaxies, respectively. Our data are connected by the solid line, while K06's are connected by the dotted line. The K06 data are plotted separately for the two survey fields.

4. Clustering Analysis

4.1. Angular Correlation

We derive the angular correlation function (ACF) separately for the sBzKs and pBzKs. We do not, however, show the results of the pBzKs, since reliable measurements are not obtained due to their small sample size (56 objects).

We first measure the ACF of sBzKs for the NW and SW subregions independently with angular bins of $\log\theta[''] = 0.4$, using the estimator given in Landy & Szalay (1993). Random data with 50000 points are used. Errors in the measurements are estimated by the bootstrap resampling method (Ling et al. 1986; Mo et al. 1992). Then the measurements for each subregion are corrected for the integral constraint, on the assumption that the true ACF obeys a power law of $w(\theta) \propto \theta^{-0.8}$. Finally, the measurements from the two subregions are averaged to obtain the ACF of sBzKs in the SDF (Figure 4).

The amplitude of the ACF, A, is obtained from a fit of $w(\theta) = A\theta^{-0.8}$ to the data, and is given in Table 2. Our sBzKs have $A = 0.58 \pm 0.13$ [arcsec$^{0.8}$], where the errors correspond to the range in which the increase in χ^2 from the best-fit value is less than unity. Our ACF measurement for sBzKs could suffer from cosmic variance, since each of the two sub-fields is only about 10 Mpc a side at $z = 2$. A survey of a larger area is clearly required to obtain results robust against possible variance. However, we infer that the amplitude of the cosmic variance in our sample will not be intolerably large, since the ACFs from the two sub-fields agree within the statistical errors, and since the number counts of our sBzKs are consistent with those of K06.

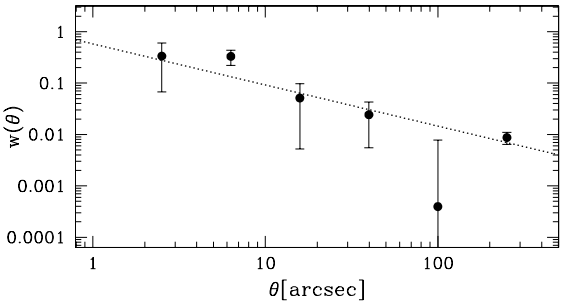

Fig. 4.— The angular correlation function of sBzKs. The error bars correspond to the 1σ errors obtained from bootstrap resampling. The dotted line is the best-fit power law of $A\theta^{-0.8}$.

4.2. Bright Samples by K06

Figure 5 shows the observed ACF amplitude against limiting K magnitude. The filled circle represents the amplitude of our sBzKs, while the six filled triangles correspond to the amplitudes for the six samples of K06 with different limiting magnitudes over $K = 20.4$ and 21.9. The ACF amplitude of sBzKs is found to decrease rapidly with decreasing K brightness. The brightest samples of K06 have $A \simeq 15$ – 20 arcsec$^{0.8}$, which is about 30 times higher than ours.

In the next subsection, the spatial correlation lengths, r_0, are calculated from the ACF amplitudes to discuss the clustering of sBzKs in real space. For the reader's reference, the three shaded regions in Figure 5 indicate, respectively, the expected ACF amplitude for $r_0 = 3$, 10 and 20 $[h^{-1}\mathrm{Mpc}]$ calculated using the redshift distribution for sBzKs adopted in the next subsection (Gaussian with $z_c = 1.9$ and $\sigma_z = 0.35$); for each r_0, the spread in amplitude corresponds to the adopted uncertainty in the σ_z of ± 0.1.

4.3. Spatial Correlation Length of sBzKs

The correlation length, r_0, for sBzKs can be calculated from the amplitude of the ACF, A, using Limber's equation (Limber 1953; Peebles 1980) if their redshift distribution is known.

4.3.1. Redshift Distribution of sBzKs

The redshift distribution, $N(z)$, of sBzKs has not been established even for bright objects with $K < 22$ owing to the lack of a large, flux-limited spectroscopic sample. In this study, we assume that the $N(z)$ of sBzKs is not dependent on K magnitude, and adopt a Gaussian distribution as a simple approximation. We determine the central redshift, z_c, and the standard deviation, σ_z, of the Gaussian as follows.

First, we use a preliminary result of the $N(z)$ of sBzKs (81 objects, most of which are $K = 21-22$) obtained from a K-selected spectroscopic survey in the EIS Deep3A field with VLT/VIMOS down to $K = 22.0$ (E. Daddi, private communication) to determine z_c and infer σ_z. This is probably the most reliable measurement of the $N(z)$ of sBzKs at present because it is based on the largest spectroscopic sample. We fit a Gaussian to this $N(z)$ after removing a strong spike at $z \sim 1.5$ (which could be due to large-scale structure) and limiting the redshift range to $1.0 < z < 3.0$, and obtain $z_c = 1.9$ and $\sigma_z = 0.4$. From this result, we adopt $z_c = 1.9$ for our Gaussian distribution. Note that the Limber transformation is insensitive to the change in z_c; for example, changing z_c by ± 0.2 around 1.9 changes r_0 only by 2.5 %.

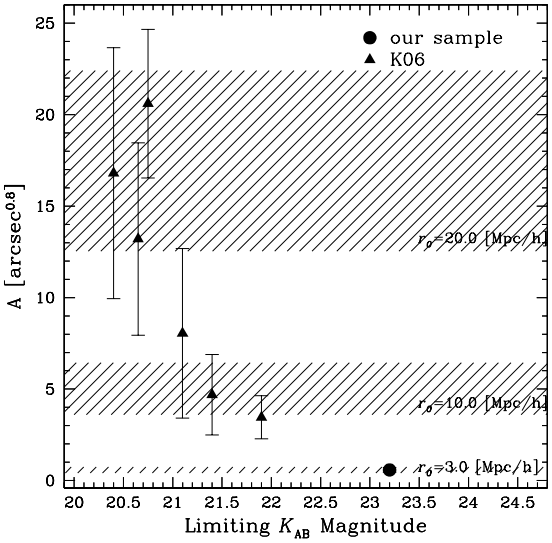

Fig. 5.— Amplitude of the ACF, A, as a function of limiting K total magnitude. The filled circle shows the measurement for our sample, while the filled triangles correspond to the six samples with different limiting magnitudes over $K = 20.4$ and 21.9 given in K06. The amplitudes for $r_0 = 20, 10$ and $3h^{-1}$Mpc calculated using the adopted redshift distribution for sBzKs (Gaussian with $z_c = 1.9$ and $\sigma_z = 0.35$) are shown by the shaded regions, whose width corresponds to the adopted uncertainty in σ_z of ± 0.1. See subsection 4.3.1 for details.

Next, we determine σ_z and express the uncertainty in our Gaussian distribution by the range of σ_z. We adopt $\sigma_z = 0.35 \pm 0.1$ for the following reasons. We find that, for a fixed A value, the range of r_0 corresponding to the range $0.25 < \sigma_z < 0.45$ covers not only the r_0 value calculated using the raw $N(z)$ from the EIS Deep3A field, but also from those given in Daddi et al. (2004) and Reddy et al. (2005). Here, the data of Reddy et al. (2005) are another measurement

of the redshift distribution based on a large sample, although the sample is not K-limited but optically selected and thus could be biased toward UV bright objects. We also find that the best-fit Gaussian parameters for the redshift distribution data of Daddi et al. (2004) and Reddy et al. (2005) are similar to the values we adopt above. Figure 6 compares the adopted Gaussian function with the $N(z)$ of Daddi et al. (2004).

It is true that a Gaussian distribution is not an excellent approximation to the existing $N(z)$ data, especially for the preliminary result of Daddi et al. (private communication) with a large spike. However, it will be reasonable to expect that the true $N(z)$ derived from a sample large enough to smooth out statistical noise and cosmic variance is not so far from a Gaussian centered at $z \sim 2$, since the isolation of $1.4 < z < 2.5$ galaxies from others using the BzK selection will not be perfect. It may be worth noting that Lyman-break galaxies, which are also selected in a two-color plane, are known to have a Gaussian-like distribution (Yoshida et al. 2006). Our purpose is not to infer the true distribution but to find a reasonable expression of it which can be used in the Limber transformation. In this sense, the adopted Gaussian and uncertainty, $z_c = 1.9$ and $\sigma = 0.35 \pm 0.1$, are a reasonable parameterization, since they include all the variations in the existing redshift distribution measurements in terms of resultant r_0 values. It is also found that the r_0 value calculated using a top-hat redshift distribution of $1.4 < z < 2.5$ (ideal selection function for BzKs) falls within the r_0 range defined by the adopted uncertainty in the Gaussian.

Finally, we should note that our assumption that the $N(z)$ does not depend on K magnitude must be tested using a future spectroscopic follow-up, although the observation of Reddy et al. (2005) may support this assumption. They derived $N(z)$ for $K < 21.8$ and $K > 21.8$ (with a limiting magnitude of $K = 24.3$) separately, which are found not to be largely different.

4.3.2. Spatial Correlation Length

The correlation length of our sBzKs derived in this manner is $r_0 = 3.2^{+0.6}_{-0.7}$ [h^{-1}Mpc] in comoving units (see also Table 2). The errors in r_0 are calculated by summing up in quadrature the errors from the measurement of A and the errors due to the adopted uncertainty in σ_z (± 0.1).

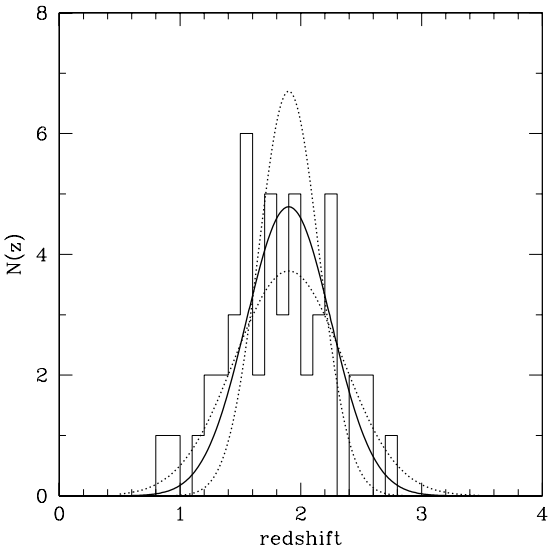

Fig. 6.— The redshift distribution of sBzKs. The histogram represents the distribution of 28 sBzKs with a spectroscopic redshift given in Daddi et al. (2004). The solid curve indicates a Gaussian distribution function with $z_c = 1.9$ and $\sigma_z = 0.35$ used to calculate the correlation length. The two Gaussians with $\sigma_z = 0.25$ and 0.45 are plotted by the dotted line to show the adopted uncertainty in the redshift distribution. The amplitude of the Gaussians has been normalized so that their areas be equal to the area of the histogram.

Figure 7 shows the correlation lengths for our sBzK sample and the six samples of K06.[1] It is found from Figure 7 that r_0 increases rapidly with increasing K brightness. The brightest sample of K06 has $r_0 \simeq 20\ h^{-1}$Mpc, which is six times larger than that of ours.

[1]The errors in r_0 of the samples of K06 are not very large in spite of the small sample sizes, because brighter sBzKs are clustered more strongly and thus have stronger signals. This in turn means that larger samples are required to measure the angular correlation function for fainter objects with the same uncertainty.

Table 2: Numbers, ACF amplitudes, correlation lengths, and dark-halo masses of sBzKs in our sample and K06's

	Field	$K_{\rm lim}$	N	A[arcsec$^{0.8}$]	$r_0[h^{-1}{\rm Mpc}]$	$\langle M_{\rm DH}\rangle[M_\odot]$	$M_{\rm DH}^{\rm min}[M_\odot]$
this work	SDF	23.2	1092	0.58±0.13	$3.2^{+0.6}_{-0.7}$	$2.8^{+4.2}_{-2.3}\times10^{11}$	$1.0^{+1.8}_{-0.9}\times10^{11}$
K06	Daddi-F	20.4	21	16.8±6.86	$21^{+5.2}_{-6.2}$	$1.6^{+0.9}_{-0.9}\times10^{14}$	$1.1^{+0.9}_{-0.6}\times10^{14}$
		20.7	43	13.2±5.26	$18^{+4.5}_{-5.4}$	$1.1^{+0.8}_{-0.6}\times10^{14}$	$8.0^{+6.0}_{-5.0}\times10^{13}$
		21.1	92	8.05±4.63	$14^{+4.4}_{-5.7}$	$6.4^{+4.6}_{-4.8}\times10^{13}$	$4.2^{+4.8}_{-3.4}\times10^{13}$
	Deep3A-F	20.7	27	20.6±4.06	$23^{+4.1}_{-4.7}$	$1.9^{+0.8}_{-0.8}\times10^{14}$	$1.5^{+0.6}_{-0.6}\times10^{14}$
		21.4	129	4.69±2.20	$10^{+2.8}_{-3.4}$	$2.8^{+2.4}_{-2.0}\times10^{13}$	$1.6^{+1.7}_{-1.3}\times10^{13}$
		21.9	387	3.46±1.18	$8.5^{+2.0}_{-2.3}$	$1.8^{+1.4}_{-1.2}\times10^{13}$	$9.0^{+9.0}_{-6.3}\times10^{12}$

5. Discussion

5.1. Masses of Dark Haloes Hosting sBzKs

The standard CDM model predicts that at any redshifts more massive dark haloes are on average more clustered (e.g., Mo & White 2002). We use the clustering strengths of our sBzK sample and those of K06 to infer the masses of their hosting haloes in the following manner. First, for an sBzK sample with a given limiting magnitude, we derive the amplitude of the spatial correlation function at 8 h^{-1} Mpc, $\xi_{\rm sBzK}(8h^{-1}{\rm Mpc})$, from the observed r_0 assuming $\xi_{\rm sBzK}\propto r^{-1.8}$. We then calculate the effective bias parameter, $b_{\rm eff}$, from

$$b_{\rm eff}=\sqrt{\frac{\xi_{\rm sBzK}(8h^{-1}{\rm Mpc})}{\xi_{\rm DM}(8h^{-1}{\rm Mpc})}}, \qquad (1)$$

where $\xi_{\rm DM}$ is the predicted correlation function of dark matter at $z=2$. Finally, we use the analytic formula of dark-halo biasing given in Sheth et al. (2001) to obtain the mass of dark haloes hosting the sBzKs.

We consider two definitions of halo mass, (i) average mass and (ii) minimum mass. Average mass, $\langle M_{\rm DH}\rangle$, is defined by:

$$b_{\rm eff}=b(\langle M_{\rm DH}\rangle), \qquad (2)$$

where $b(M_{\rm DH})$ is the bias parameter of haloes with mass $M_{\rm DH}$. We regard $\langle M_{\rm DH}\rangle$ as the typical halo mass of the sample. Minimum mass, $M_{\rm DH}^{\rm min}$, is defined through:

$$b_{\rm eff}=\frac{\int_{M_{\rm DH}^{\rm min}}^{\infty}b(M_{\rm DH})n(M_{\rm DH})dM_{\rm DH}}{\int_{M_{\rm DH}^{\rm min}}^{\infty}n(M_{\rm DH})dM_{\rm DH}}, \qquad (3)$$

where $n(M_{\rm DH})dM_{\rm DH}$ is the mass function of dark haloes. In this definition, $M_{\rm DH}^{\rm min}$ corresponds to the mass of haloes hosting the faintest galaxies in the sample (In this paper we assume that bias increases monotonically with galaxy brightness).

Our definition of $M_{\rm DH}^{\rm min}$ can be regarded as a simplification of the halo model approach which uses three parameters including $M_{\rm DH}^{\rm min}$ to model galaxy clustering (Berlind & Weinberg 2002; Bullock et al. 2002; Moustakas & Somerville 2002; Hamana et al. 2004); the other two parameters are used to model the mass dependence of the number of galaxies per halo. In this study, we do not adopt this approach, but place a constraint only on $M_{\rm DH}^{\rm min}$ for simplicity, since this approach requires an accurately measured ACF shape with small angular bin sizes.

The average dark-halo mass of our sBzK sample is estimated to be $\langle M_{\rm DH}\rangle\simeq3\times10^{11}M_\odot$. In contrast, the sBzKs of K06 samples are found to be hosted by massive haloes with $\langle M_{\rm DH}\rangle\simeq2\times10^{13}$ – $2\times10^{14}M_\odot$.

The difference between $\langle M_{\rm DH}\rangle$ and $M_{\rm DH}^{\rm min}$ is less than factor 3. This is because fainter objects are more numerous, thus contributing more to the overall clustering of the sample. For the readers' reference, The dotted horizontal lines of Figure 7 indicate $M_{\rm DH}^{\rm min}$ as a function of r_0.

These results show that sBzKs reside in dark haloes with a mass range of as wide as three orders of magnitude, $10^{11-14}M_\odot$, with fainter objects being found in less massive haloes. Typical haloes hosting faint sBzKs ($K<23.2$) are several times less massive than that of the Milky Way ($M_{\rm DH}\simeq(1-2)\times10^{12}M_\odot$: e.g., Sakamoto et al.

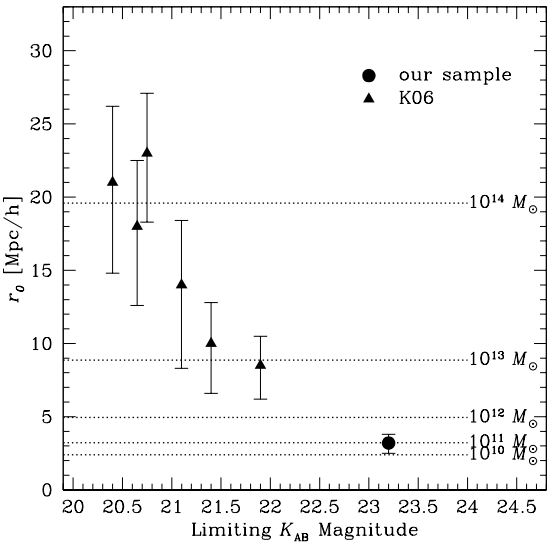

Fig. 7.— Correlation length, r_0, as a function of limiting K total magnitude. The filled circle shows the measurement for our sample, while the filled triangles correspond to the six samples with different limiting magnitudes over $K = 20.4$ and 21.9 given in K06. The dotted horizontal lines indicate the minimum mass of dark haloes inferred from r_0.

(2003)) while those hosting bright sBzKs with limiting magnitudes of $K = 20.4$ to 21.9 have masses comparable to those of present-day galaxy groups and clusters.

5.2. Ratio of Stellar Mass to Dark Halo Mass

We estimate the minimum stellar mass, which corresponds to that of the faintest galaxies in the sample, for our sample and the six samples of K06 from the K magnitude and $z' - K$ color of the faintest object in each sample, using equations (6) and (7) given in Daddi et al. (2004). These equations were derived using bright sBzKs which have accurate stellar masses based on a fit of model spectra to multicolor data. Daddi et al. (2004) found the typical error in mass estimates from these equations to be $\Delta \log M_\star = 0.2$.

Figure 8 plots the minimum stellar mass of sBzKs against the minimum mass of their hosting haloes. The minimum stellar mass of our sample is $M_\star^{\rm min} \simeq 1 \times 10^{10} M_\odot$, while those of K06 are three to ten times higher. On the other hand, the minimum dark-halo mass of our sample is $M_{\rm DH}^{\rm min} \simeq 1 \times 10^{11} M_\odot$, while those of K06 are two to three orders of magnitude higher. It is thus concluded that dark-halo mass increases more rapidly than the stellar mass of individual sBzKs residing in the halo.

We note that the stellar-mass estimation for our sample is less reliable than that for K06. Equations (6) and (7) in Daddi et al. (2004) have not been tested for faint sBzKs like those in our sample, which may have systematically different stellar populations and dust extinctions. The observed trend of increasing $M_{\rm DH}^{\rm min}/M_\star^{\rm min}$ with $M_\star^{\rm min}$ will disappear if the $M_\star^{\rm min}$ of our sample is overestimated by more than factor ten, although such a large overestimation seems to be unlikely.

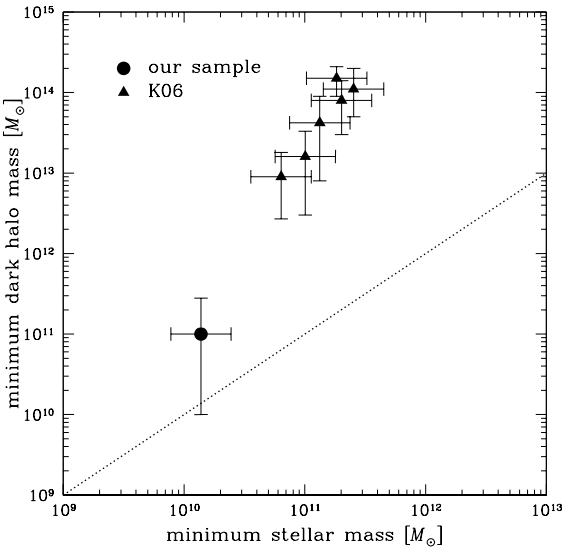

Fig. 8.— Minimum dark-halo mass plotted against minimum stellar mass for sBzKs. The filled circle indicates our sample, while the filled triangles correspond to the six samples with different limiting magnitudes given in K06. Minimum stellar masses correspond to the limiting magnitudes of the samples.

5.3. Halo Occupation Number

The halo occupation number of a given class of galaxies is defined as the average number of this class of galaxies hosted in a single dark halo. We estimate the halo occupation number of sBzKs for two magnitude limits, $K < 23.2$ and $K < 21.9$, using our sample and the faintest sample of K06, and then examine whether or not occupation number depends on luminosity.

The halo occupation number for sBzKs with $K = 23.2$ is estimated by dividing the number density of our sBzKs by that of dark haloes hosting them, i.e., haloes more massive than $M_{\rm DH}^{\rm min}$. We have 1092 objects in a survey volume of $7.1 \times 10^5 {\rm Mpc}^3$. This leads to a number density of 2.4×10^{-3} ${\rm Mpc}^{-3}$ after correction for detection completeness of a modest amount. The number density of dark haloes is calculated to be $1.7 \times 10^{-2} {\rm Mpc}^{-3}$ from the analytic formula of the halo mass function given by Sheth et al. (2001). Thus, the halo occupation number of sBzKs with $K < 23.2$ is estimated to be $\simeq 0.1$.

Similarly, we use the faintest sample of K06 with $K < 21.9$ to estimate the halo occupation number to be $\simeq 4$.[2] Here, the number of sBzKs in this sample is 387, the survey volume is $3.2 \times 10^{-4} {\rm Mpc}^{-3}$, and the number density of the hosting haloes is $7.5 \times 10^{-5} {\rm Mpc}^{-3}$.

These two estimates show that the occupation number of sBzKs increases strongly with increasing halo mass. Haloes with $M_{\rm DH} \gtrsim 10^{13} M_\odot$ have several sBzKs on average, while only one tenth (on average) of haloes with $M_{\rm DH} \gtrsim 10^{11} M_\odot$ host an sBzK. It is reasonable that haloes with $\gtrsim 10^{13} M_\odot$ host multiple sBzKs, since they are as massive as present-day groups and clusters of galaxies. On the other hand, the very small occupation number for haloes with $\gtrsim 10^{11} M_\odot$ may imply that they are not massive enough to always feed a galaxy more luminous than $K = 23.2$.

[2]We do not use the brighter five samples of K06, because sBzKs in them are hosted by more massive haloes, whose number densities, and thus occupation numbers, have increasingly large errors owing to a steep slope of the mass function.

5.4. Comparison of r_0 between sBzKs and Other Objects

Figure 9 compares the correlation lengths of sBzKs with those of various types of objects from present-day early-type galaxies and clusters of galaxies, up to galaxies at $z = 4$. The five curves show the correlation lengths of dark haloes with five fixed $M_{\rm DH}^{\rm min}$ values as a function of redshift. Haloes with a fixed minimum mass have larger r_0 at higher z because b increases with z for any $M_{\rm DH}$.

It is found from Figure 9 that at $z \sim 2$ faint ($K < 23.2$) sBzKs and BX/BM galaxies have similar correlation lengths and thus similar dark-halo masses of the order of $\sim 10^{11} M_\odot$. This result is in accord with the recent claim by Reddy et al. (2005) that a high fraction (70 – 80%) of BXs/BMs with $22.3 < K < 22.8$ are also selected as sBzKs and that the fraction increases with decreasing K brightness. Therefore, faint sBzKs and BXs/BMs are largely overlapping subsets of star-forming galaxies at $z \sim 2$ hosted by relatively low-mass haloes. In Figure 9, LBGs at $z = 3 - 4$ have also similar masses to faint sBzKs, while haloes hosting QSOs are on average an order of magnitude more massive.

Brighter sBzKs with $K \simeq 21 - 22$ are found to have as large correlation lengths, $r_0 \simeq 10 - 15\ h^{-1}$ Mpc, as DRGs at $z \sim 2 - 3$ and EROs at $z \sim 1 - 2$. They are located in haloes as massive as the order of $M_{\rm DH} \sim 10^{13} M_\odot$. Their correlation lengths partly overlap with those of present-day luminous early-type galaxies and clusters. Large fractions of DRGs and EROs are known to be passive galaxies, while sBzKs are star-forming galaxies. This implies that haloes with similar masses can host galaxies with extremely different star-formation properties. Brightest sBzKs with $K < 21$ are most strongly clustered among the high-z populations plotted here. Their correlation lengths are comparable to or even larger than those of present-day rich clusters.

5.5. Present-day Descendants of sBzKs

We use the extended Press-Schechter formalism (Bond et al. 1991; Bower 1991) to predict the mass of the present-day descendants of dark haloes hosting sBzKs at $z \sim 2$. We find that haloes at $z = 2$ with a mass equal to the $\langle M_{\rm DH} \rangle$ of faint

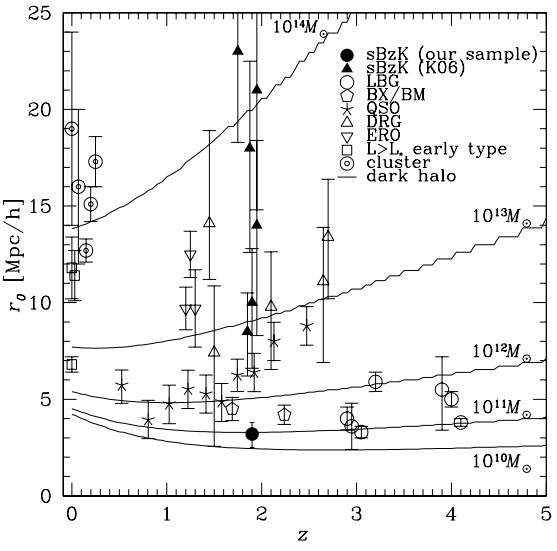

Fig. 9.— Correlation lengths of various types of objects over $0 \leq z \leq 4$. The filled symbols represent sBzKs; circle: our sample, triangles: K06. The other symbols indicate the measurements for other objects taken from the literature; open circles: LBGs at $z \sim 3$ ($23.5 < R < 25.5$, Adelberger et al. (2005); $20.0 < I < 24.5$, Foucaud et al. (2003)) and $z \sim 4$ ($i' < 25, 26, 27.5$, Ouchi et al. (2005)), open pentagons: BX/BM galaxies with $23.5 < R < 25.5$ at $z \sim 2$ (Adelberger et al. 2005), stars: QSOs at $z \sim 0.5$ — 2 ($18.25 < b_J < 20.85$, Croom et al. (2005)), open triangles: Distant Red Galaxies (DRGs) at $z \sim 2$ — 3 ($K_{\rm Vega} < 21$, Quadri et al. (2006); $K < 20.7$, Foucaud et al. (2006); $K < 23.5$, Grazian et al. (2006)), open inverted triangles: Extremely Red Objects (EROs) at $z \sim 1$ — 2 ($K_{\rm Vega} < 24$, Daddi et al. (2003); $K_{\rm Vega} < 22$, Roche et al. (2003); $K_{\rm Vega} < 18.4$, Brown et al. (2005)), open squares: present-day luminous early-type galaxies (Overzier et al. 2003), double circles: present-day clusters of galaxies (Bahcall et al. 2003). The five curves show the correlation length of dark haloes with five different minimum masses as labeled.

($K < 23.2$) sBzKs ($2.8 \times 10^{11} M_\odot$) will become haloes with masses of $(3.7 - 10.0) \times 10^{11} M_\odot$ at $z = 0$ (68% range of the distribution function; the extended Press-Schechter formalism can predict descendant masses only in a statistical sense).[3]

Thus, the present-day descendants of the typical haloes of faint sBzKs are likely to be less massive than that of the Milky Way. They may host sub-L^* galaxies in nearby fields. On the basis of a clustering analysis of BX/BM galaxies, Adelberger et al. (2005) concluded that BXs/BMs are progenitors of normal ellipticals in the local universe. The correlation length they obtained is $r_0 = 4.2 \pm 0.5\ h^{-1}$Mpc for BXs and $r_0 = 4.5 \pm 0.6\ h^{-1}$Mpc for BMs. These values correspond to dark haloes several times more massive than those of our faint sBzKs. Thus, their conclusion does not seem to conflict with our result obtained here.

On the other hand, haloes with a mass equal to the $\langle M_{\rm DH} \rangle$ of $K < 20.4$ sBzKs in K06 ($1.6 \times 10^{14} M_\odot$) are predicted to have $(4.3{-}9.3) \times 10^{14} M_\odot$ at present. These masses are comparable to those of most massive clusters like Coma. The number density of sBzKs with $K < 20.4$, $(1 - 2) \times 10^{-5}$Mpc^{-3}, is close to that of the present-day rich clusters more massive than $2 \times 10^{14} M_\odot$, $\sim 1 \times 10^{-5}$Mpc^{-3} (Rines et al. 2006). This suggests that brightest sBzKs are ancestors of central galaxies in rich clusters seen at present.

These calculations suggest that sBzKs evolve into galaxies over a wide range of mass (or luminosity) in a variety of environment at $z = 0$, depending on their apparent K brightness.

6. Conclusions

In this paper, we have studied clustering properties of star-forming BzK galaxies (sBzKs) at $1.4 \lesssim z \lesssim 2.5$ over a wide range of K brightness ($K < 23.2$).

We have used deep multi-color data of 180 arcmin^2 in the Subaru Deep Field to construct a sample of 1092 faint ($K < 23.2$) sBzK galaxies. We have derived the angular correlation function (ACF) of the sBzKs, and measured its amplitude to be $A = (0.58 \pm 0.13)$ [arcsec$^{0.8}$] by fitting a power law of $w(\theta) \propto \theta^{-0.8}$ to the data. We have then transformed the ACF amplitude into the correlation length assuming a Gaussian redshift distribution of $z_c = 1.9$ and $\sigma_z = 0.35 \pm 0.1$, and obtained $r_0 = 3.2^{+0.6}_{-0.7}\ h^{-1}$ Mpc. We have not been

[3]Dr. Takashi Hamana kindly provided the code to calculate the distribution function.

able to derive the ACF of passive BzKs in our data because of the small sample size. We infer from the correlation length that our sBzKs reside in haloes with an average mass of $2.8 \times 10^{11} M_{\odot}$ and a minimum mass of $1.0 \times 10^{11} M_{\odot}$.

We then have inferred dark-halo masses for six bright ($K < 21.9$) sBzK samples of K06 in the same manner. Combining our data with those of K06, we have examined how the mass of hosting dark haloes depends on the K luminosity of sBzKs. We have found that the mass of dark haloes rapidly increases with K brightness of individual sBzKs; K06's sBzKs are brighter than ours by only up to $\simeq 10$ times, but they are hosted by haloes two to three orders of magnitude more massive than the haloes of our sBzKs. The halo occupation number, the number of BzKs hosted in a dark halo, is found to be higher for brighter sBzKs.

The correlation lengths of sBzKs have been compared with those of various types of objects up to $z = 4$. We have found that faint ($K < 23.2$) sBzKs have similar r_0 values to BX/BM galaxies, which are optically-selected star-forming galaxies at $z \sim 2$. We argue that these two types of galaxies are similar populations hosted by relatively low-mass haloes with the order of $M_{\rm DH} \sim 10^{11} M_{\odot}$. On the other hand, sBzKs with $K \simeq 21 - 22$, EROs, and DRGs are found to reside in massive haloes with the order of $\sim 10^{13} M_{\odot}$. The clustering of brightest sBzKs with $K < 21$ is the strongest among the high-z populations.

Finally, we have predicted present-day descendants of haloes hosting sBzKs using the extended Press-Schechter formalism. Descendants are found to span a wide range of mass, depending on the K brightness of sBzKs in them. Typical descendants of haloes hosting sBzKs with $K < 23.2$ are less massive than the Milky Way, while those for $K < 20.4$ sBzKs are as massive as richest clusters.

We wish to thank Takashi Hamana for providing his code to compute the mass growth of dark haloes using the extended Press-Schechter formalism. We are very grateful to Emanuele Daddi for kindly providing new data of the redshift distribution of 81 sBzKs prior to publication. We also thank an anonymous referee for useful comments which have greatly improved the paper. The United Kingdom Infrared Telescope is operated by the Joint Astronomy Centre on behalf of the U.K. Particle Physics and Astronomy Council. The WFCAM data were reduced on the general common-use computer system at the Astronomy Data Center, ADC, of the National Astronomical Observatory of Japan.

REFERENCES

Adelberger, K. L., Steidel, C. C., Shapley, A. E., Hunt, M. P., Erb, D. K., Reddy, N. A., & Pettini, M. 2004, ApJ, 607, 226

Adelberger, K. L., Steidel, C. C., Pettini, M., Shapley, A. E., Reddy, N. A., & Erb, D. K. 2005, ApJ, 619, 697

Bahcall, N. A., Dong, F., Hao, L., Bode, P., Annis, J., Gunn, J. E., & Schneider, D. P. 2003, ApJ, 599, 814

Berlind, A. A, & Weinberg, D. H. 2002, ApJ, 575, 587

Bertin, E., & Arnouts, S. 1996, A&A, 117, 393

Bond, J. R., Cole, S., Efstathiou, G., Kaiser, N. 1991, ApJ, 379, 440

Bower, R. G. 1991, MNRAS, 248, 332

Brown, M. J. I., Jannuzi, B. T., Dey, A., & Tiede, G. P. 2005, ApJ, 621, 41

Bullock, J. S., Wechsler, R. H., & Somerville, R. S. 2002, MNRAS, 329, 246

Coleman, G. D., Wu, C.-C., & Weedman, D. W. 1980, ApJS, 43, 393

Croom, S. M., et al. 2005, MNRAS, 356, 415

Daddi, E., et al. 2003, ApJ, 588, 50

Daddi, E., et al. 2004, ApJ, 617, 746

Daddi, E., et al. 2005, ApJ, 626, 680

Dickinson, M., Papovich, C., Ferguson, H. C., & Budavári, T. 2003, ApJ, 587, 25

Gallazzi, A., Chrlot, S., Brinchmann, J., White, S. D. M., & Tremonti, C. A. 2005, MNRAS, 362, 41

Grazian, A., et al. 2006, A&A, 453, 507

Guhathakurta, P., Tvson, J. A., & Maiewski, S. R., 1990, ApJ, 357, L9

Gunn, J. E., & Stryker, L. L., 1983, ApJS, 52, 121

Fontana, A., et al. 2003, ApJ, 594, L9

Foucaud, S., et al. 2003, A&A, 409, 835

Foucaud, S., et al. 2006, astro-ph/0606386

Hamana, T., Ouchi, M., Shimasaku, K., Kavo, I., & Suto, Y. 2004, MNRAS, 347, 813

Kajisawa, M., & Yamada, T. 2001, PASJ, 53, 833

Kashikawa, N., et al. 2004, PASJ, 56, 1011

Kong, X., et al. 2006, ApJ, 638, 72 (K06)

Landy, S. D., & Szalay, A. S. 1993, ApJ, 412, 64

Limber, D. N. 1953, ApJ, 117, 134

Ling, E. N., Frenk, C. S., & Barrow, J. D. 1986, MNRAS, 223, L21

Maihara, T., et al. 2001, PASJ, 53, 25

Mo, H. J., Jing, Y. P., & Börner, G., et al. 1992, ApJ, 392, 452

Mo, H. J., & White, S. D. M. 2002, MNRAS, 336, 112

Moustakas, L. A., & Somerville, R. S. 2002, ApJ, 577, 1

Ouchi, M., et al. 2005, ApJ, 635, L117

Overzier, R. A., Röttgering, H. J. A., Rengelink, R. B., & Wilman, R. J. 2003, A&A, 405, 53

Peebles, P. J. E. 1980, The Large-Scale Structure of the Universe (Princeton: Princeton Univ. Press)

Quadri, R., et al. 2006, astro-ph/0606330

Reddy, N. A., Erb, D. K., Steidel, C. C., Shapley, A. E., Adelberger, K. L., & Pettini, M. 2005, ApJ, 633, 748

Richards, G. T., et al. 2006, AJ, 131, 2766

Rines, K., Diaferio, A., & Natarajan, P., 2006, astro-ph/0606545

Roche, N. D., Dunlop, J., & Almaini, O. 2003, MNRAS, 346, 803

Sakamoto, T., Chiba, M., & Beers, T. C. 2003, A&A, 397, 899

Schlegel, D. J., Finkbeiner, D. P., & Davis, M. 1998, ApJ, 500, 525

Sheth, R. K., Mo, H. J., & Tormen, G. 2001, MNRAS, 323, 1

Skrutskie, M. F., et al. 2006, AJ, 131, 1163

Steidel, C. C., Shapley, A. E., Pettini, M., Adelberger, K. L., Erb, D. K., Reddy, N. A., & Hunt, M. P. 2004, ApJ, 604, 534

Yoshida, M., et al. 2006, ApJ, 653, 988

This 2-column preprint was prepared with the AAS LaTeX macros v5.2.